Sliding Mode Control of EV Electric Differential System

A. Haddoun, M. E. H. Benbouzid, D. Diallo, R. Abdessemed, J. Ghouili and K. Srairi

***Abstract*—This paper describes the sliding mode control of an electric differential system for Electric Vehicle (EV) with two induction motor drives (one for each wheel). In this case, the electric differential will manage the speed difference between the two wheels when cornering. The proposed sliding mode control approach is evaluated on an EV global model taking into account the vehicle dynamics. Simulations have been carried out on a test vehicle propelled by two 37-kW induction motors to evaluate the consistency and the performance of the proposed control approach. The commonly used European drive cycle ECE-15 is adopted for simulation. The obtained results seem to be very promising.**

***Index Terms*—Electric vehicle, electric differential, induction motor, sliding mode control.**

I. Introduction

SINGLE drive systems for EVs generally use only one drive motor that is connected to the wheels through reduction gears and a mechanical differential. The mechanical differential is used to control the speed of the left and right wheel during steering maneuvers. Multi-drive systems can use two drive motors that directly drive the rear wheels. This provides the opportunity to improve the drive train overall efficiency and reliability by replacing the mechanical differential with an electric differential, The electric differential is then used to control the speed variation of the wheels during steering maneuvers [1].

The natural ability of electric drives to control the generated torque and the introduction of an independent control of the traction wheel drives (two or four) can allow a high performance traction control with low cost, quick response and easy to design implementation. A vehicle topology like the proposed one allows a simplified mechanical structure of the vehicle and an effective traction control will allow to reduce the energy consumption, namely by diminishing energy losses from the friction between the tires and the road surface during sliding, improving then the tires lifetime [2-3].

Manuscript received June 30, 2006.

A. Haddoun* and M.E.H. Benbouzid are with the Laboratoire d'Ingénierie Mécanique et Electrique (LIME), University of Western Brittany, Rue de Kergoat – BP 93169, 29231 Brest Cedex 3, France (phone: +33 2 98 01 80 07; fax: +33 2 98 01 66 43; e-mail: m.benbouzid@ieee.org). *A. Haddoun is also with the University of Oum El Bouaghi, 04000 Oum El Bouaghi, Algeria.

D. Diallo is with the Laboratoire de Génie Electrique de Paris (LGEP) CNRS UMR 8507, University of Paris XI, Supélec, Plateau du Moulon, 91192 Gif-Sur-Yvette, France (e-mail: ddiallo@ieee.org).

R. Abdessemed is with the University of Batna, 05000 Batna, Algeria.

J. Ghouili is with the GRET Research Group, Engineering Faculty, University of Moncton, Moncton, New Brunswick, Canada.

K. Srairi is with the University of Biskra, 07000 Biskra, Algeria.

However, one of the main issues in the design of this vehicle (without mechanical differential) is to assume the car stability. During normal driving condition, all the drive wheel system requires a symmetrical distribution of torque in both sides. This symmetrical distribution is not sufficient when the adherence coefficient of tires is changing: the wheels have different speeds; so the needs for traction control system [4]. This is still an open problem as illustrated by a limited available literature [5-7].

To address this open problem, this paper proposes a sliding mode control approach of an electrical differential system for an EV propelled by two induction motor drives (one for each wheel). The induction motor model which is suitable for sliding mode control is derived in the rotor flux reference frame. A nonlinear switching surface is proposed based on the existence of a certain positive definite function. Moreover, the proposed control approach takes into account the vehicle aerodynamics, and is not applied to the sole induction motors. It should be noted that the induction motor has been adopted for the EV propulsion because it seems to be the candidate that better fulfils the major requirements for EVs propulsion [8].

II. The Vehicle Model

A. Nomenclature

v	=	Vehicle speed;
α	=	Grade angle;
P_{te}	=	Vehicle driving power;
F_{te}	=	Tractive force;
F_{rr}	=	Rolling resistance force;
F_{hc}	=	Hill climbing force;
F_{la}	=	Acceleration force;
F_{wa}	=	Angular acceleration force;
μ_{rr1}	=	Tire rolling resistance coefficient for mass ($0.005 < \mu_{rr1} < 0.4$);
μ_{rr2}	=	Tire rolling resistance coefficient for speed ($0.056 < \mu_{rr2} < 0.4$);
m	=	Vehicle mass;
g	=	Gravitational acceleration constant;
ρ	=	Air density;
C_{ad}	=	Aerodynamic drag coefficient ($0.2 < C_{ad} < 0.4$);
A	=	Vehicle frontal area;
v_0	=	head-wind velocity;
a	=	Vehicle acceleration;
J	=	Total inertia (rotor and load);
ω	=	Motor angular speed;
T_L	=	Load torque;
T_m	=	Motor torque;
G	=	Gear ratio;
η_g	=	Gear system efficiency;
r	=	Tire radius.

B. Dynamics Analysis

Based on principles of vehicle mechanics and aerodynamics, one can assess both the driving power and energy necessary to ensure vehicle operation [9-11].

1) Road load and tractive force. The first step in vehicle performance modeling is to derive an equation for the tractive effort. This is the force propelling the vehicle forward and transmitted to the ground through the wheels. Consider a vehicle of mass *m*, moving at a speed *v*, up an angle α slope, as shown in Fig. 1. The tractive effort has to accomplish the following: overcome the rolling resistance, overcome the aerodynamic drag, overcome the vehicle weight, and accelerate the vehicle if the speed is not constant.

The rolling resistance F_{rr} is primarily due to the friction of the vehicle tire on the road. The rolling resistance is approximately constant, and hardly depends on vehicle speed.

$$F_{rr} = \mu_{rr1} mg + \mu_{rr2} N_r v \tag{1}$$

The main factors affecting μ_{rr1} are the tire type and pressure. Typical values are 0.015 for a radial ply tire, down to about 0.005 for tires developed especially for electric vehicles. Concerning μ_{rr2}, typical value for EVs is about 0.056.

Aerodynamic drag F_{ad} is the viscous resistance of air acting upon the vehicle. This force is due to the friction of the vehicle body moving through the air. It is function of the frontal area, the shape, protrusions such as side mirrors, ducts and air passages, spoilers, etc.

$$F_{ad} = \frac{1}{2}\rho C_{ad} A \left(v + v_0\right)^2 \tag{2}$$

The force needed to drive the vehicle up a slope is the most straightforward to find. It is simply the component of the vehicle weight that acts along the slope.

$$F_{hc} = \pm mg \sin\alpha \tag{3}$$

If the velocity of the vehicle is changing, then an additional force is needed. This force will provide the linear acceleration of the vehicle.

$$F_{la} = ma \tag{4}$$

However, for a more accurate representation of the needed force to accelerate the vehicle, we should also consider rotational acceleration as well as linear acceleration. The main issue here is the electric motor, not necessarily because of its particularly high moment of inertia, but because of its higher angular speeds.

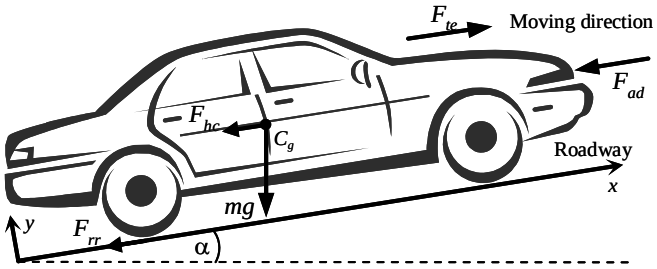

Fig. 1. Elementary forces acting on a vehicle.

Referring to Fig. 2, we can derive the following

$$T_m = \frac{F_{te}\ r}{G} \Rightarrow F_{te} r = \frac{G}{r} T_m \tag{5}$$

The motor torque required for this angular acceleration is

$$T_m = JG \frac{a}{r} \tag{6}$$

Then, the acceleration force is derived using (5)

$$F_{wa} = \frac{G}{r} T_m \Rightarrow F_{wa} = J \frac{G^2}{r^2} a \tag{7}$$

We must note that in these simple equations we have assumed that the gear system is 100% efficient. Since the system will usually be very simple, the efficiency is often very high. However, it will never be 100%. We should therefore refine (7) by incorporating the gear system efficiency η_g. The required force will be slightly larger.

$$F_{wa} = J \frac{G^2}{\eta_g r^2} a \tag{8}$$

The total tractive effort is then given by

$$F_{te} = F_{rr} + F_{ad} + F_{hc} + F_{la} + F_{wa} \tag{9}$$

It should be noted that F_{la} and F_{wa} will be negative if the vehicle is slowing down and that F_{hc} will be negative if it is going downhill.

2) Motor ratings and transmission. The power required to drive a vehicle at a speed *v* has to compensate counteracting forces.

$$P_{te} = vF_{te} = v(F_{rr} + F_{ad} + F_{hc} + F_{la} + F_{wa}) \tag{10}$$

III. Induction Motor Modeling

A. Nomenclature

V_{ds} (V_{qs})	=	*d*-axis (*q*-axis) stator voltages;
i_{ds} (i_{qs})	=	*d*-axis *q*-axis) stator currents;
λ_{dr} (λ_{qr})	=	*d*-axis (*q*-axis) rotor flux linkages;
R_s (R_r)	=	Stator (rotor) resistance;
L_s (L_r)	=	Stator (rotor) inductance;
L_m	=	Magnetizing inductance;
L_σ	=	Leakage inductance ($L_\sigma = L_s - L_m^2/L_r$);
$\omega_e(\omega_r)$	=	Stator (rotor) electrical speed;

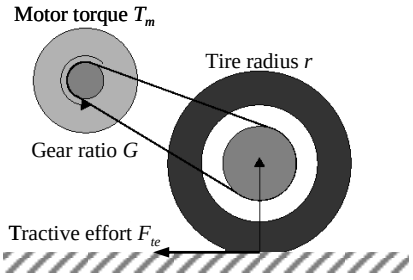

Fig. 2. A simple arrangement for connecting a motor to a driving wheel.

Ω = Rotor speed (ω_r/p);
ω_{sl} = Slip frequency, $\omega_{sl} = \omega_s - \omega_r$
B = Motor damping ratio;
p = pole-pair number.

$$\begin{cases} k_1 = \dfrac{R_s}{L_\sigma} + \dfrac{R_r L_m^2}{L_r^2 L_\sigma}, \; k_2 = \dfrac{R_r L_m}{L_r^2 L_\sigma}, \; k_3 = \dfrac{L_m}{L_r L_\sigma}, \\ k_4 = \dfrac{R_r L_m}{L_r}, \; k_5 = \dfrac{R_r}{L_r}, \; k_6 = \dfrac{1}{L_\sigma}, \; k_t = \dfrac{3}{2} p \dfrac{L_m}{L_r} \end{cases}$$

B. Induction Motor Dynamic Model

As we intend to use sliding mode control, the induction motor model, which is suitable in this case, should be derived in the rotor flux reference frame. Therefore, the induction motor dynamic model in the *d-q* synchronously rotating frame with rotor flux is described by (11)-(13) [12].

$$\frac{d}{dt}\begin{bmatrix} i_{ds} \\ i_{qs} \\ \lambda_{dr} \\ \lambda_{qr} \end{bmatrix} = \begin{bmatrix} -k_1 & \omega_e & k_2 & \omega_r k_3 \\ -\omega_e & -k_1 & -\omega_r k_3 & k_2 \\ k_4 & 0 & -k_5 & \omega_{sl} \\ 0 & k_4 & -\omega_{sl} & -k_5 \end{bmatrix} \begin{bmatrix} i_{ds} \\ i_{qs} \\ \lambda_{dr} \\ \lambda_{qr} \end{bmatrix} + k_6 \begin{bmatrix} V_{ds} \\ V_{qs} \\ 0 \\ 0 \end{bmatrix} \tag{11}$$

$$\frac{d\omega_r}{dt} = -\frac{B}{J}\omega_r - \frac{1}{J}(T_m - T_L) \tag{12}$$

$$T_m = k_t\left(\lambda_{dr} i_{qs} - \lambda_{qr} i_{ds}\right) \tag{13}$$

IV. Sliding Mode Control

A. Why Sliding Mode Control?

Sliding mode control is one of the effective nonlinear robust control approaches since it provides system dynamics with an invariant property to uncertainties once the system dynamics are controlled in the sliding mode [13]. It has been introduced to the area of power electronics and electric drives because of rapid dynamic response and tough robustness. By interpreting the torque ripple as a disturbance and the nonlinearity as a gain variation, a sliding mode control is expected to cope with the problems troubling the induction motor drives without necessitating the knowledge of the motor characteristics. Moreover, a sliding mode control should give the induction motor drives the usual benefits of insensitivity to the drive parameter variations and disturbances [14].

B. The Sliding Mode Controller

A sliding mode exists, if in the vicinity of the switching surface, $S(x) = 0$, the velocity vectors of the state trajectory always point toward the switching surface. The design of the controller is based on the determination of switched feedback gains that will drive the system state trajectory to the switching surface and maintain a sliding mode condition [13].

The proposed sliding mode control is designed on the basis of rotor flux field orientation with following definitions:

$$\begin{cases} \lambda_{qr} = 0 \\ \lambda_{dr} = \lambda = constant \end{cases} \tag{14}$$

Using (14), one can derive from (11)-(13) the following (induction motor dynamics).

$$\begin{cases} \dfrac{di_{ds}}{dt} = -k_1 i_{ds} + \omega_e i_{qs} + k_2 \lambda_r + k_6 V_{ds} \\ \dfrac{di_{qs}}{dt} = -k_1 i_{qs} - \omega_e i_{ds} - k_2 \lambda_r + k_6 V_{qs} \\ \dfrac{d\lambda_r}{dt} = -k_5 \lambda_r + k_4 i_{ds} \\ T_e = k_t \lambda_r i_{qs} \end{cases} \tag{15}$$

The following definitions are introduced

$$\begin{cases} \dfrac{di_{ds}}{dt} = -k_1 i_{ds} + u_d \\ \dfrac{di_{qs}}{dt} = -k_1 i_{qs} + u_q \end{cases} \tag{16}$$

in order to extract the desired voltage commands.

$$\begin{cases} u_d = -Usign(S_d) \\ u_q = -Usign(S_q) \end{cases} \tag{17}$$

Where U is the control gain, S_d and S_q are the selected sliding surfaces corresponding to errors between stator currents and their references.

$$\begin{cases} S_d = e_{ids} = (i_{ds}^* - i_{ds}) \\ S_q = e_{iqs} = (i_{qs}^* - i_{qs}) \end{cases} \tag{18}$$

These commands have been also selected as (17) for Lyapunov stability requirements [13-14].

Time derivative of (18) gives current errors dynamics.

$$\begin{cases} \dot{e}_{ids} = \dfrac{dS_d}{dt} = k_1 i_{ds} + Usign(S_d) + \dfrac{di_{ds}^*}{dt} \\ \dot{e}_{iqs} = \dfrac{dS_q}{dt} = k_1 i_{qs} + Usign(S_q) + \dfrac{di_{qs}^*}{dt} \end{cases} \tag{19}$$

The stability of the proposed controller is proven using the following Lyapunov candidate function [13].

$$V = \frac{1}{2}\left(S_d^2 + S_q^2\right) \tag{20}$$

Hence sliding mode arises on the intersection of both surfaces $S_d = 0$ and $S_q = 0$, which enables one to steer the variables under control to the desired values. In our case, stator currents converge to their reference values.

V. The Electric Differential and Its Implementation

Figure 3 illustrates the implemented system (electric and mechanical components) in the Matlab-Simulink® environment.

The proposed control system principle could be summarized as follows: *(1)* A current loop, based on sliding mode control, is used to control each motor torque; *(2)* The speed of each rear wheel is controlled using speeds difference feedback.

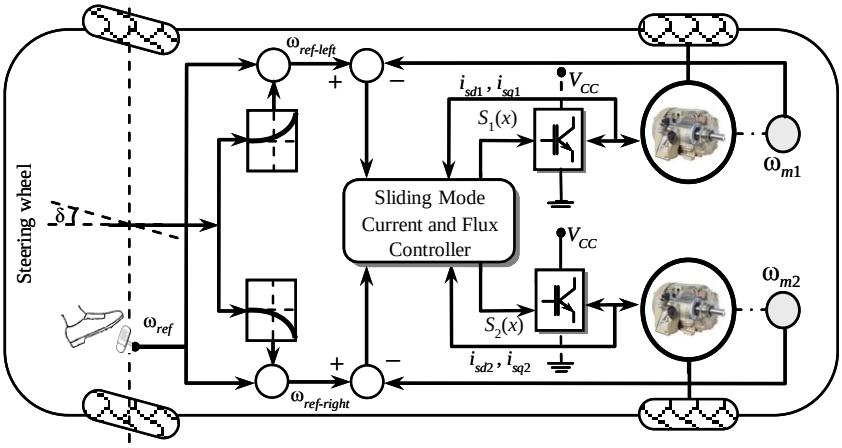

Fig. 3. EV propulsion and control systems schematic diagram.

Since the two rear wheels are directly driven by two separate motors, the speed of the outer wheel will require being higher than the speed of the inner wheel during steering maneuvers (and vice-versa). This condition however can be easily met if a position encoder is used to sense the angular position of the steering wheel. The common reference speed ω_{ref} is then set by the accelerator pedal command. The actual reference speed for the left drive $\omega_{ref\text{-}left}$ and the right drive $\omega_{ref\text{-}right}$ are then obtained by adjusting the common reference speed ω_{ref} using the output signal from the position encoder. If the vehicle is turning right, the left wheel speed is increased and the right wheel speed remains equal to the common reference speed ω_{ref}. If the vehicle is turning left the right wheel speed is increased and the left wheel speed remains equal to the common reference speed ω_{ref} [6].

Usually, a driving trajectory is quite enough for an analysis of the vehicle system model. We have therefore adopted the Ackermann-Jeantaud steering model as it is widely used as driving trajectory. In fact, Ackermann steering geometry is a geometric arrangement of linkages in the steering of a car or other vehicle designed to solve the problem of wheels on the inside and outside of a turn needing to trace out circles of different radii. Modern cars do not use pure Ackermann-Jeantaud steering, partly because it ignores important dynamic and compliant effects, but the principle is sound for low speed maneuvers [15]. It is illustrated in Fig. 4.

From this model, the following characteristic can be calculated.

$$R = \frac{L}{\tan\delta} \tag{21}$$

Where δ is the steering angle. Therefore, each wheel drive linear speed is given by

$$\begin{cases} V_1 = \omega_V \left(R - d/2 \right) \\ V_2 = \omega_V \left(R + d/2 \right) \end{cases} \tag{22}$$

and their angular speed by

$$\begin{cases} \omega_{1mes} = \dfrac{L - (d/2)\tan\delta}{L}\omega_V \\ \omega_{2mes} = \dfrac{L + (d/2)\tan\delta}{L}\omega_V \end{cases} \tag{23}$$

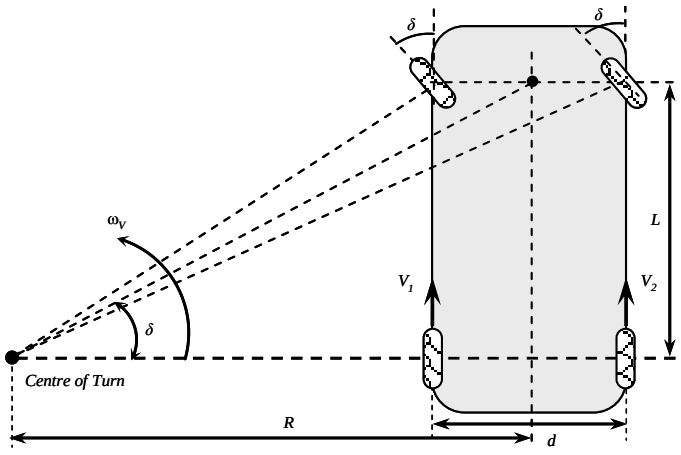

Fig. 4. Driving trajectory model.

The difference between wheel drive angular speeds is then

$$\Delta\omega = \omega_{1mes} - \omega_{2mes} = -\frac{d\tan\delta}{L}\omega_V \tag{24}$$

and the steering angle indicates the trajectory direction.

$$\begin{cases} \delta > 0 \Rightarrow Turn\ left \\ \delta = 0 \Rightarrow Straight\ ahead \\ \delta < 0 \Rightarrow Turn\ right \end{cases} \tag{25}$$

In accordance with the above described equation, Fig. 5 show the electric differential system block diagram as used for simulations.

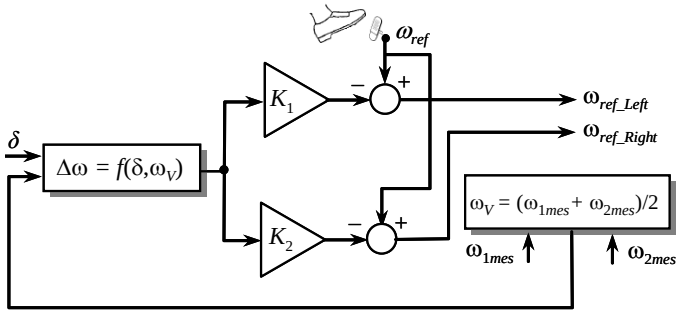

Fig. 5. Block diagram of the electric differential system.

VI. Simulation Results

Numerical simulations have been carried out, on an EV propelled by two 37-kW induction motor drives which ratings are summarized in the appendix. In the appendix are also given the electrical vehicle mechanical and aerodynamic characteristics. The objectives of the carried out simulations are to assess the efficiency and dynamic performances of the proposed sliding mode control strategy.

The test cycle is the urban ECE-15 cycle (Fig. 6) [16]. A driving cycle is a series of data points representing the vehicle speed versus time. This driving cycle represents urban driving. It is characterized by low vehicle speed (maximum 50 km/h) and is useful for testing small electrical vehicles performance.

The electric differential performance are first illustrated by Fig. 7 that shows each wheel drive speeds during steering for $0 < t < 1180$ sec. It is obvious that the electric differential operates satisfactorily.

Figures 8 and 9 illustrate the EV dynamics, respectively, the flux (λ_{dr}) in each induction motor and the developed torque on the left and right wheel drives, with changes in the acceleration pedal position (Fig 10) and a varied road profile (rising and downward portions). It should be noticed that flux and torque variations are as large as are the variations of the accelerator pedal and the road profile.

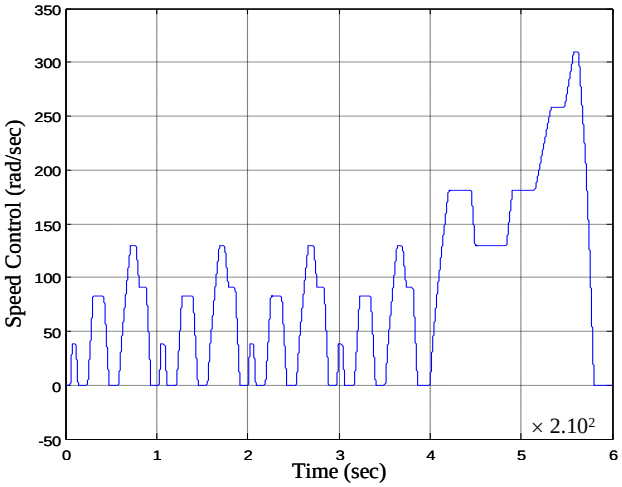

Fig. 6. European urban driving schedule ECE-15.

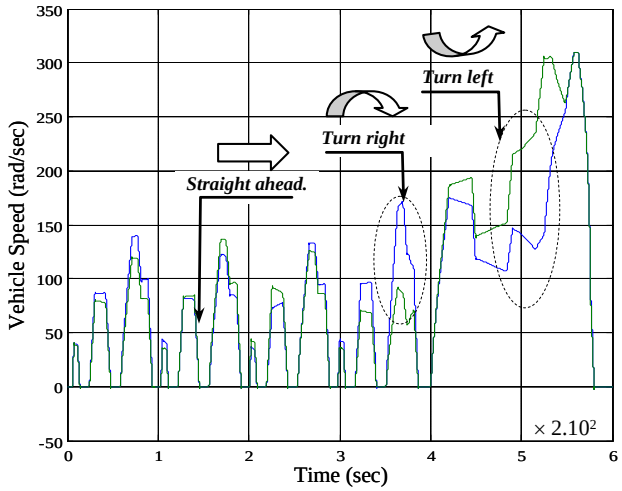

Fig. 7. Vehicle wheels speed.

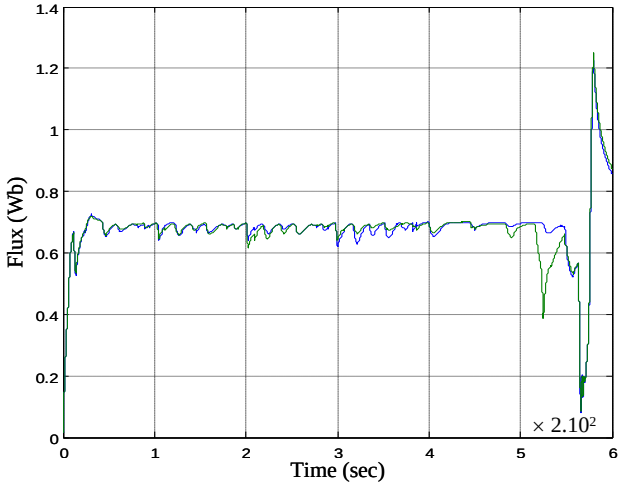

Fig. 8. Flux λ_{dr}.

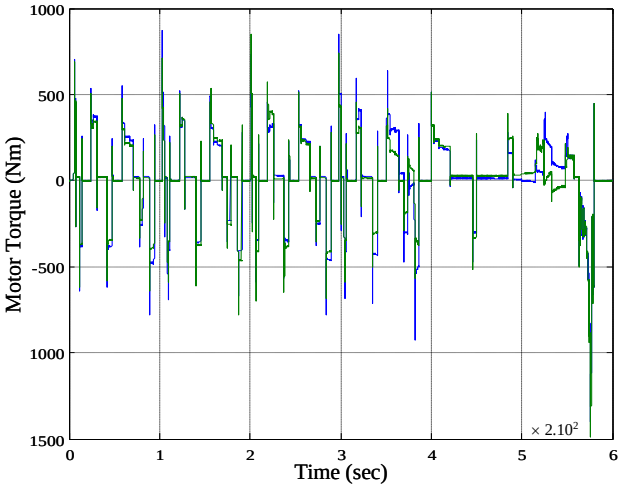

Fig. 9. Motor torque.

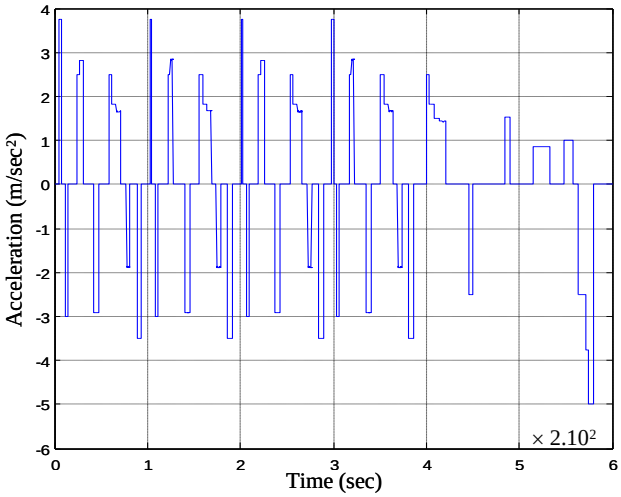

Fig. 10. Acceleration pedal position.

Figure 11 illustrates the power required to move the EV. To find the power taken from the battery to provide the tractive, we have to be able to find various efficiencies at all operating points.

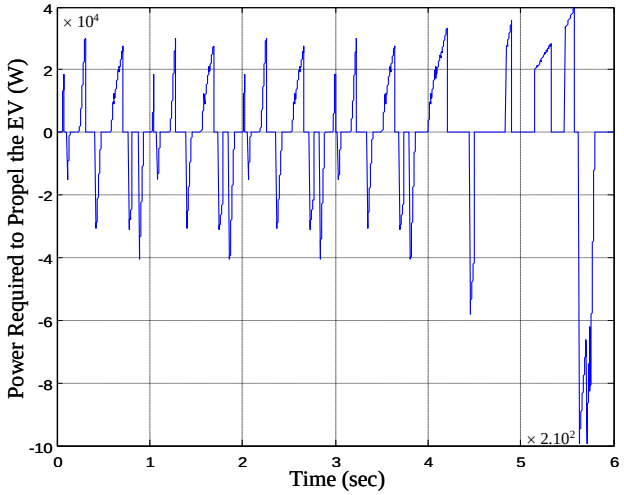

Fig. 11. Power required to propel the EV.

VII. Conclusion

In this paper, a sliding mode traction control algorithm for an electrical vehicle with two separate wheel drives has been proposed. This algorithm is necessary to improve the EV steerability and stability during trajectory changes. An electrical differential was implemented and take account of the speed difference between the two wheels when cornering. Moreover, as traction control systems impose a very precise knowledge of the vehicle dynamics, a vehicle dynamics model was exhaustively detailed and applied.

Numerical simulations have been carried out, on an EV propelled by two 37-kW induction motor drives. The test cycle was in our case the urban ECE-15 cycle. During traction and regenerative braking, a correlation of traction control with motor performances has been realized. The obtained results seem to be very promising.

Appendix

Rated Data of the Simulated Induction Motor

37 kW, 50 Hz, 400/230 V, 64/111 A, 24.17 Nm, 2960 rpm
R_s = 85.1 mΩ, R_r = 65.8 mΩ
L_s = 31.4 mH, L_r = 29.1 mH, L_m = 29.1 mH
J = 0.23 kg.m²

EV Mechanical and Aerodynamic Parameters

m = 1540 kg (two 70 kg passengers), A = 1.8 m^2, r = 0.3 m
μ_{rr1} = 0.0055, μ_{rr2} = 0.056, C_{ad} = 0.19
G = 104, η_g = 0.95
T = 57.2 Nm (stall torque)
v_0 = 4.155 m/sec
g = 9.81 m/sec^2, ρ = 0.23 kg/m^3

References

[1] C.C. Chan et *al.*, "An overview of power electronics in electric vehicles," *IEEE Trans. Industrial Electronics*, vol. 44, n°1, pp. 3-13, February 1997.

[2] A.W. Divelbiss et *al.*, "Trajectory tracking control of a car-trailer system," *IEEE Trans. Control Systems Technology*, vol. 5, n°3, pp. 269-278, May 1997.

[3] B. Arnet et *al.*, "Torque control on electric vehicles with separate wheel drives," in *Proceedings of EPE'97*, vol. 4, pp. 659-664, September 1997.

[4] S. Sakai et *al.*, "Motion control in an electric vehicle with four independently driven in-wheel motors," *IEEE/ASME Trans. Mechatronics*, vol. 4, n°1, pp.9-16, March 1996.

[5] G. Tao et *al.*, "A novel driving and control system for direct-wheel-driven electric vehicle," *IEEE Trans. Magnetics*, vol. 41, n°1, pp. 497-500, January 2005.

[6] S. Gair and *al.*, "Electronic differential with sliding mode controller for a direct wheel drive electric vehicle," i*n Proceedings of IEEE ICM'04*, pp. 98-103, June 2004.

[7] L. Ju-Sang et *al.*, "A neural network model of electric differential system for electric vehicle," *in Proceedings of IEEE IECON'00*, vol. 1, pp. 83-88, October 2000.

[8] M.E.H. Benbouzid et *al.*, "Electric motor drive selection issues for HEV propulsion systems: A comparative study," *IEEE Trans. Vehicular Technology*, September 2006.

[9] A. Haddoun et *al.*, "A loss-minimization DTC scheme for EV induction motors," *IEEE Trans. Vehicular Technology*, December 2006.

[10] I. Husain et *al.*, "Design, modeling and simulation of an electric vehicle system," *SAE Technical Paper Series*, Paper # 1999-01-1149.

[11] J. Larminie, *Electric Vehicle Technology Explained*. Wiley: Oxford, 2003.

[12] A. Benchaïb et *al.*, "Real-time sliding mode observer and control of induction motor," *IEEE Trans. Industrial Electronics*, vol. 46, n°1, pp. 128-138, February 1999.

[13] K.D. Young et *al.*, "A control engineer's guide to sliding mode control," *IEEE Trans. Control Systems Technology*, vol. 7, n°3, pp. 328-342, May 1999.

[14] V. I. Utkin, "Sliding mode control design principles and applications to electric drives," *IEEE Trans. on Industrial Electronics*, vol. 40, n°1, pp. 23-36, February 1993.

[15] R.E. Colyer et *al.*, "Comparison of steering geometries for multi-wheeled vehicles by modelling and simulation," *in Proceedings of IEEE CDC'98*, vol. 3, pp. 3131-3133, December 1998.

[16] M. André et *al.*, "Driving cycles for emissions measurements under European Conditions," *SAE Paper*, # 950926, In *Global Emission Experiences: Processes, Measurements, and Substrates (SP-1094)*, Warrendale (USA), pp. 193-205, 1995.